Inorg. Chem. **2007**, *46*, 9602–9608

Cu–Pd–Cu and Cu–Pt–Cu Linear Frameworks: Synthesis, Magnetic Properties, and Theoretical Analysis of Two Mixed-Metal Complexes of Dipyridylamide (dpa), Isostructural, and Isoelectronic with $[Cu_3(dpa)_4Cl_2]^+$

Isiah Po-Chun Liu,[†,‡] Gene-Hsiang Lee,[†] Shie-Ming Peng,*[,†,‡] Marc Bénard,[§] and Marie-Madeleine Rohmer*[,§]

Laboratoire de Chimie Quantique, Institut de Chimie, UMR 7177, CNRS-ULP, Strasbourg, France, Department of Chemistry, National Taiwan University, Taipei 10764, Taiwan, Republic of China, Institute of Chemistry, Academia Sinica, Taipei, Taiwan ROC

Received February 19, 2007

The synthesis and crystal structure of two heteronuclear compounds stabilized by four dipyridylamide (dpa) ligands is reported. $Cu_2Pd(dpa)_4Cl_2$ (**1**) and $Cu_2Pt(dpa)_4Cl_2$ (**2**) exhibit an approximate D_4 symmetry and a linear metal framework. They are structurally similar to the homotrinuclear complexes $M_3(dpa)_4L_2$ already characterized with various transition metals (M = Cr, Co, Ni, Cu, Rh, Ru). With 26 metal valence electrons, they are also isoelectronic to the oxidized form of the tricopper complex $[Cu_3(dpa)_4Cl_2]^+$ (**3**), previously characterized and investigated by Berry et al.[10] The magnetic properties and the EPR spectra of **1** and **2** are reported. The results for **1** are interpreted in terms of a weak antiferromagnetic interaction ($2J = -7.45$ cm^{-1} within the framework of the Heisenberg Hamiltonian $\hat{H} = -2J_{AB}\,\hat{S}_A\hat{S}_B$) between the Cu(II) magnetic centers. For **2**, the antiferromagnetic interaction sharply decreases to <1 cm^{-1}. These properties are at variance with those of (**3**), for which a relatively strong antiferromagnetic interaction ($2J = -34$ cm^{-1}) had been reported. DFT/UB3LYP calculations reproduce the decrease of the magnetic interaction from **3** to **1** and assign it to the role of the nonmagnetic metal in the transference of the superexchange coupling. However, the vanishing of the magnetic interaction in **2** could not be reproduced at this level of theory and is tentatively assigned to spin–orbit coupling.

Introduction

Polypyridylamide anions and their derivatives are multidentate ligands, characterized by an alternation of pyridine and amido ends. They have become of current use to stabilize linear frameworks of transition metals, in which adjacent metals are at bonding distance from each other. 1D complexes of that sort have been characterized with a large variety of metals, that is, chromium, cobalt, nickel, copper, ruthenium, and rhodium.[1] In spite of the rather rigid character of the polypyridylamide ligand coating, structural and magnetic properties of these complexes appear to be quite versatile and can be tuned as a function of the length of the metal string;[2] of the type of axial ligands terminating this string;[3] of the nature of the nitrogen ends, pyridine or amido,[4,5] coordinating the metals in the terminal position;

* To whom correspondence should be addressed. E-mail: mmrohmer@quantix.u-strasbg.fr (M.-M.R.), smpeng@ntu.edu.tw (S.-M.P.).
† National Taiwan University.
‡ Academia Sinica.
§ Laboratoire de Chimie Quantique.

(1) (a) Berry, J. F. In *Multiple Bonds between Metal Atoms*, 3rd ed.; Cotton, F. A., Murillo, C. A., Walton, R. A., Eds; Springer-Science and Business Media, Inc.: New-York, 2005. (b) Bera, J. K.; Dunbar, K. R. *Angew. Chem., Int. Ed.* **2002**, *41*, 4453. (c) Zhu, L.-G.; Peng, S.-M. *Wuji Huaxue Xuebao*, **2002**, *18*, 117. (d) Yeh, C.-Y.; Wang, C.-C.; Chen, C.-h.; Peng, S.-M. In *Nano Redox Sites: Nano-Space Control and its Applications*; Hirao, T., Ed.; Springer: Berlin, 2006; Chapter 5, pp 85−117.
(2) Peng, S.-M.; Wang, C.-C.; Jang, Y.-L.; Chen, Y.-H.; Li, F.-Y.; Mou, C.-Y.; Leung, M.-K. *J. Magn. Magn. Mater.* **2000**, *209*, 80.
(3) (a) Wang, C.-C.; Lo, W.-C.; Chou, C.-C.; Lee, G.-H.; Chen, J.-M.; Peng, S.-M. *Inorg. Chem.* **1998**, *37*, 4059. (b) Yeh, C.-Y.; Chiang, Y.-L.; Peng, S.-M. *Inorg. Chem.* **2002**, *41*, 4096. (c) Tsao, T.-B.; Lee, G.-H.; Peng, S.-M. *Dalton Trans.* **2003**, 1465. (d) Sheng, T.; Appelt, R.; Comte, V.; Vahrenkamp, H. *Eur. J. Inorg. Chem.* **2003**, 3731. (e) Berry, J. F.; Cotton, F. A.; Lu, T.; Murillo, C. A.; Roberts, B. K.; Wang, X. *J. Am. Chem. Soc.* **2004**, *126*, 7082. (f) Berry, J. F.; Cotton, F. A.; Murillo, C. A. *Organometallics* **2004**, *23*, 2503. (g) Berry, J. F.; Cotton, F. A.; Murillo, C. A; Roberts, B. K. *Inorg. Chem.* **2004**, *43*, 2277. (h) Cotton, F. A.; Chao, H.; Murillo, C. A.; Wang, X. *Dalton Trans.* **2006**, 5416.

10.1021/ic070319l CCC: $37.00
Published on Web 10/11/2007

and of the presence of electron-attractor substituents in the vicinity of these nitrogen ends.[5] These various channels are presently being explored to gain control over the structural, magnetic, and conductive properties of these 1D complexes in the perspective of their use as molecular wires or other devices in nanoelectronics.[6−8] The recent characterization of $Co_2Pd(dpa)_4Cl_2$, exhibiting the first heterometallic framework in this family of complexes,[9] has opened new possibilities to extend the scope of their properties. In the present work, we present two new heterotrimetallic complexes of dpa, $Cu_2Pd(dpa)_4Cl_2$ (**1**), and $Cu_2Pt(dpa)_4Cl_2$ (**2**), which are isostructural and isoelectronic to the oxidized form of the tricopper complex, $[Cu_3(dpa)_4Cl_2]^+$ (**3**), previously characterized in Cotton's group.[10] X-ray structures, magnetic susceptibility, and EPR spectra have been determined for **1** and **2**, which have been concurrently modeled by means of DFT calculations.

Experimental and Computational Section

Materials. All of the reagents, Hdpa, and solvents were purchased from commercial sources and were used as received unless otherwise noted.

[CuPdCu(dpa)$_4$Cl$_2$] (1) and [CuPtCu(dpa)$_4$Cl$_2$] (2). Ligand Hdpa (0.68 g, 4 mmol), $CuCl_2$ (0.27 g, 2 mmol), K_2MCl_4 (M = Pd: 0.33 g, M = Pt: 0.42 g; 1 mmol), and 40 g naphthalene (as solvent) were placed in an Erlenmeyer flask. After stirring the mixture at 150 °C during 2 h for palladium, 3 h for platinum, *t*-BuOK (0.44 g, 4 mmol) in *t*-BuOH (20 mL) was added dropwise. The resulting solution was then stirred during an additional 2 h for palladium, 3 h for platinum. After cooling the mixture to 80 °C, hexane was added, and the resulting precipitate was filtered out. The solid was extracted with CH_2Cl_2, and the solution was then layered with diethyl ether. After 1 week for M = palladium and 3 weeks for M = platinum, green crystals of $[CuMCu(dpa)_4Cl_2]$ formed. For (**1**): Yield : 0.49 g, 50%. MS(FAB) m/z: 985 ($[CuPdCu(dpa)_4Cl_2]^+$), UV−vis (CH_2Cl_2) λ_{max}/nm ($\epsilon/10^4$ M^{-1} cm^{-1}): 319 (6.01), 393 (2.18), 429 (1.58). For (**2**): Yield: 0.19 g, 18%. MS(FAB) m/z: 1073 ($[CuPtCu(dpa)_4Cl_2]^+$), 1038 ($[CuPtCu(dpa)_4Cl]^+$), 1002 ($[CuPtCu(dpa)_4]^+$), UV/vis (CH_2Cl_2) λ_{max}/nm ($\epsilon/10^4$ M^{-1} cm^{-1}): 339 (7.28), 372 (3.5), 400 (2.67).

Elemental analysis results: For $[CuPdCu(dpa)_4Cl_2]$ Anal. Calcd for $C_{40}H_{32}Cl_2Cu_2N_{12}Pd$: C, 48.77; H, 3.27; N, 17.06. Found: C, 47.89; H, 3.41; N, 16.57.

Table 1. Crystallographic Data for $CuPdCu(dpa)_4Cl_2$ (**1**) and $CuPtCu(dpa)_4Cl_2$ (**2**)

	1·ether	**2**·ether
formula	$C_{44}H_{42}Cl_2Cu_2N_{12}OPd$	$C_{44}H_{42}Cl_2Cu_2N_{12}OPt$
fw	1059.28	1147.97
space group	$P2_1/c$	$P2_1/c$
cryst syst	monoclinic	monoclinic
a, (Å)	16.1125(2)	16.1109(2)
b, (Å)	15.7610(2)	15.7691(2)
c, (Å)	16.9971(2)	16.9970(2)
α, (deg)	90	90
β, (deg)	99.2852(5)	99.1356(9)
γ, (deg)	90	90
V, Å^3	4259.84(9)	4263.39(9)
Z	4	4
T, (K)	150(2)	150(2)
radiation *λ*, (Å)	0.71073	0.71073
ρ_{calcd}, (g cm^{-3})	1.652	1.788
$R1^a$, $wR2^b$ ($I > 2\sigma I$)	0.0309, 0.0743	0.0495, 0.1028
$R1^a$, $wR2^b$ (all data)	0.0491, 0.0824	0.1146, 0.1212

[a] $R1 = \sum||F_o| - |F_c||/\sum|F_o|$. [b] $wR2 = \{\sum[w(F_o^2 - F_c^2)^2]/\sum[w(F_o^2)^2]\}^{1/2}$, with $w = 1/\sigma^2(F_o^2) + (aP)^2 + bP$, $P = (F_o^2 + 2F_c^2)/3$.

For $[CuPtCu(dpa)_4Cl_2]$ Anal. Calcd for $C_{44}H_{42}Cl_2Cu_2N_{12}OPt$: C, 46.04; H, 3.69; N, 14.64. Found: C, 47.06; H, 3.82; N, 15.03.

Physical Measurements. Magnetic susceptibility was collected by a Quantum external magnetic field of 3000 G. FAB mass spectra were taken on a JEOL HX-110 HF double-focusing spectrometer operating in the positive ion detection mode. Electronic spectra of **1** and **2** in CH_2Cl_2 were measured in a range of 250−2500 nm on a PerkinElmer Lambda 900 UV−vis-NIR Spectrometer. EPR spectra were monitored with a Bruker EMX-10. Samples were run at 9.49 GHz (X-band) at 4 K.

X-ray Structure Determinations. Crystallographic data were collected at 150(2)K on a NONIUS Kappa CCD diffractometer using graphite-monochromatized Mo Kα radiation (λ = 0.71073 Å). Cell parameters were retrieved and refined using *DENZO-SMN* software on all observed reflections. Data reduction was performed with the *DENZO-SMN* software.[11] An empirical absorption was based on the symmetry-equivalent reflection and absorption corrections were applied with the *SORTAV* program.[12] The crystallographic data of **1** and **2** are collected in Table 1. The structures were solved and refined with *SHELX* programs.[13] The hydrogen atoms were included in calculated positions and refined using a riding mode.

DFT Calculations. Calculations and geometry optimizations on **1**, **2**, and **3** have been carried out using the Density Functional Theory (DFT) formalism with the spin unrestricted option, as implemented in the *Gaussian03* software,[14] with the B3LYP exchange-correlation functional. All-electron valence double-ζ basis sets (D95V) were used to describe carbon, nitrogen, and hydrogen atoms. Los Alamos core potentials were used to model the neon cores of chlorine and copper and the *n*s, *n*p, and *n*d cores of heavier metal atoms (n = 3 for palladium, n = 4 for platinum). The valence shell of chlorine and all types of metal atoms was described at the double-ζ level (LanL2DZ basis). The antiferromagnetic low-spin state of **1** and **2** has been characterized and its geometry optimized using the broken symmetry (BS) approach first proposed by Ginsberg[15] and then developed by Noodleman.[16] The exchange parameter $2J_{AB}$ between two magnetic centers A and B is defined

(4) (a) Lai, S.-Y.; Lin, T.-W.; Chen, Y.-H.; Wang, C.-C.; Lee, G.-H.; Yang, M-h.; Leung, M.-k. Peng, S.-M. *J. Am. Chem. Soc.* **1999**, *121*, 250. (b) Cotton, F. A.; Daniels, L. M.; Lei, P.; Murillo, C. A.; Wang, X. *Inorg. Chem.,* **2001**, *40*, 2778. (c) López, X.; Huang, M.-Y.; Huang, G.-C.; Peng, S.-M.; Li, F.-Y.; Bénard, M.; Rohmer, M.-M. *Inorg. Chem.* **2006**, *45*, 9075.

(5) López, X.; Bénard, M.; Rohmer, M.-M. *Inorg. Chem.* **2007**, *46*, 5.

(6) Berry, J. F.; Cotton, F. A.; Murillo, C. A. *Dalton Trans.* **2003**, 3015.

(7) Huang, M.-Y.; Yeh, C.-Y.; Lee, G.-H.; Peng, S.-M. *Dalton Trans.* **2006**, 5683.

(8) (a) Lin, S.-Y.; Chen, I-W. P.; Chen, C.-h.; Hsieh, M.-H.; Yeh, C.-Y.; Lin, T.-W.; Chen, Y.-H.; Peng, S.-M. *J. Phys. Chem. B* **2004**, *108*, 959. (b) Chae, D.-H.; Berry, J. F.; Jung, S.; Cotton, F. A.; Murillo, C. A.; Yao, Z. *Nano Lett.* **2006**, *6*, 165. (c) Chen, I-W. P.; Fu, M.-D.; Tseng, W.-H.; Yu, J.-H.; Wu, S.-H.; Ku, C.-J.; Chen, C.-h.; Peng, S.-M. *Angew. Chem., Int. Ed.* **2006**, *45*, 5814.

(9) Rohmer, M.-M.; Liu, I. P.-C.; Lin, J.-C.; Chiu, M.-J.; Lee, C.-H.; Lee, G.-S.; Bénard, M.; López, X.; Peng, S.-M. *Angew. Chem., Int. Ed.* **2007**, *46*, 3533.

(10) Berry, J. F.; Cotton, F. A.; Daniels, L. M.; Murillo, C. A.; Wang, X. *Inorg. Chem.* **2003**, *42*, 2418.

(11) Otwinowski, Z.; Minor, W. In *Methods in Enzymology: Macromolecular Crystallography, Part A*; Carter Jr, C. W., Sweet, R. M., Eds.; Academic Press: San Diego, 2005; Vol. 276.

(12) Blessing, R. H. *Acta Crystallogr., Sect. A* **1995**, 33.

(13) Sheldrick, G. M. *SHELXL-97, Program for the Solution of Crystal Structures*; University of Göttingen: Göttingen, Germany, 1997.

as follows by the Heisenberg−Dirac-van Vleck (HDVV) Hamiltonian:[17]

$$\hat{H}^{HDVV} = -2J_{AB}\hat{S}_A\hat{S}_B \quad (1)$$

whose eigenvalues are associated with the relative energies $E^T = -2J_{AB}$ and $E^S = 0$ for $S_A = S_B = {}^1/_2$.

Because the energy ^{BS}E of the single-determinant broken-symmetry solution is not a pure-spin state but a weighted average of the energies of the pure-spin multiplets,[16c,18] the energy of the true singlet should be deduced from the difference $^{BS}E - {}^{T}E$ by means of an appropriate spin projection procedure. Within the DFT framework, however, the projection approach is controversial. Ruiz et al.[19] argue that the unprojected BS state represents the best approximation to the real antiferromagnetic state within the single determinant Kohn−Sham theory. It is indeed clear that the unprojected results are in most cases closer to experimental values, including for the present complexes. However, we persist in using projected energy values because they provide a lower bound to the true energy[20] and have the merit of attracting attention to the importance of overlap between magnetic orbitals. We used the approximate projection proposed by Yamaguchi et al., valid for 2 and 3 magnetic centers,[21] which relies on the dependence of J_{AB} upon the spin contamination of the BS solution:

$$2J_{AB} = 2({}^{BS}E - {}^{HS}E) / ({}^{HS}\langle S^2\rangle - {}^{BS}\langle S^2\rangle) \quad (2)$$

$^{HS}\langle S^2\rangle$ and $^{BS}\langle S^2\rangle$ denote the total spin angular momentum calculated in the high spin and in the broken symmetry solutions, respectively. In case of a negligible overlap between the magnetic orbitals, $^{BS}\langle S^2\rangle$ is close to a maximal value $\langle S^2\rangle_{max}$, which is equal to 1.0 when $S_A = S_B = {}^1/_2$. In **1**, **2**, and **3**, $^{BS}\langle S^2\rangle$ was indeed found very close to 1.0, which means that projection increases the computed values of J_{AB} by a factor of ∼2. All of the geometry optimizations have been carried out on the high spin (triplet) state, with the constraints of the D_4 point group. The energy of the BS state was computed assuming the *same* geometry ($E_{BS//HS}$). Separate geometry optimizations for the HS and for the BS states leading to an adiabatic energy difference directly comparable to experiment should, in principle, eliminate the bias in favor of the state for which the geometry optimization has been carried out.[22] This bias could be neglected, however, for energy separations amounting to a few cm^{-1}, when the calculation of the adiabatic energy difference leads to chaotic results stemming from the small energy oscillations still occurring at the convergence cutoff values.

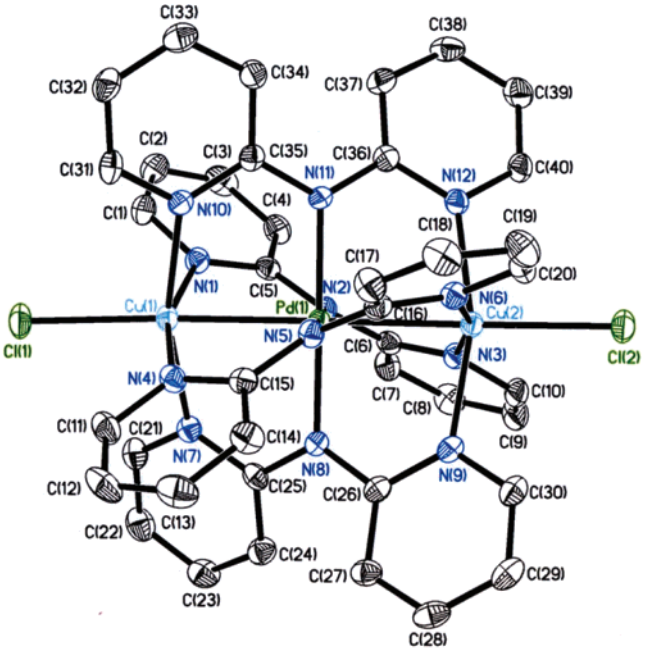

Figure 1. Molecular structure of **1**. Ellipsoids are drawn at 50% probability level. Hydrogen atoms and interstitial solvents have been omitted for clarity.

Results and Discussion

Structures of 1 and 2. **1** and **2** are isomorphous and crystallize in the monoclinic system with space group $P2_1/c$. The ORTEP diagram of **1** is shown in Figure 1. The diagram of **2** is quite similar and is displayed in the Supporting Information (Figure S1). Selected geometrical parameters are listed in Table 2 for **1** and **2** and compared with computed values. The crystal structures of both complexes look very much alike and resemble that of the isoelectronic, homonuclear complex $[Cu_3(dpa)_4Cl_2]^+$ (**3**).[10] In all three complexes, the metal chains are helically wrapped by four dpa ligands. The coordination environments of the terminal copper atoms form distorted square pyramids with

(14) Frisch, M. J.; Trucks, G. W.; Schlegel, H. B.; Scuseria, G. E.; Robb, M. A.; Cheeseman, J. R.; Montgomery, J. A., Jr.; Vreven, T.; Kudin, K. N.; Burant, J. C.; Millam, J. M.; Iyengar, S. S.; Tomasi, J.; Barone, V.; Mennucci, B.; Cossi, M.; Scalmani, G.; Rega, N.; Petersson, G. A.; Nakatsuji, H.; Hada, M.; Ehara, M.; Toyota, K.; Fukuda, R.; Hasegawa, J.; Ishida, M.; Nakajima, T.; Honda, Y.; Kitao, O.; Nakai, H.; Klene, M.; Li, X.; Knox, J. E.; Hratchian, H. P.; Cross, J. B.; Bakken, V.; Adamo, C.; Jaramillo, J.; Gomperts, R.; Stratmann, R. E.; Yazyev, O.; Austin, A. J.; Cammi, R.; Pomelli, C.; Ochterski, J. W.; Ayala, P. Y.; Morokuma, K.; Voth, G. A.; Salvador, P.; Dannenberg, J. J.; Zakrzewski, V. G.; Dapprich, S.; Daniels, A. D.; Strain, M. C.; Farkas, O.; Malick, D. K.; Rabuck, A. D.; Raghavachari, K.; Foresman, J. B.; Ortiz, J. V.; Cui, Q.; Baboul, A. G.; Clifford, S.; Cioslowski, J.; Stefanov, B. B.; Liu, G.; Liashenko, A.; Piskorz, P.; Komaromi, I.; Martin, R. L.; Fox, D. J.; Keith, T.; Al-Laham, M. A.; Peng, C. Y.; Nanayakkara, A.; Challacombe, M.; Gill, P. M. W.; Johnson, B.; Chen, W.; Wong, M. W.; Gonzalez, C.; Pople, J. A. *Gaussian 03*, revision C.02; Gaussian, Inc.: Wallingford, CT, 2004.
(15) Ginsberg, A. P. *J. Am. Chem. Soc.* **1980**, *102*, 111.
(16) (a) Noodleman, L. *J. Chem. Phys.* **1981**, *74*, 5737. (b) Noodleman, L.; Baerends, E. J. *J. Am. Chem. Soc.* **1984**, *106*, 2316. (c) Noodleman, L.; Davidson, E. R. *Chem. Phys.* **1986**, *109*, 131. (d) Noodleman, L.; Norman, J. G., Jr.; Osborne, J. H.; Aizman, A.; Case, D. A. *J. Am. Chem. Soc.* **1985**, *107*, 3418. (e) Noodleman, L.; Case, D. A.; Aizman, A. *J. Am. Chem. Soc.* **1988**, *110*, 1001. (f) Noodleman, L.; Peng, C. Y.; Case, D. A.; Mouesca, J. M. *Coord. Chem. Rev.* **1995**, *144*, 199.
(17) (a) Dirac, P. A. M. *Proc. R. Soc. London, Ser. A* **1926**, *112*, 661; **1929**, *123*, 714. (b) Heisenberg, W. *Z. Phys.* **1926**, *38*, 411. (c) van Vleck, J. H. *Theory of Electric and Magnetic Susceptibilities*; Oxford University Press: London, 1932. (d) Kahn, O. *Molecular Magnetism*; Wiley-VCH: New York, 1993.
(18) (a) Illas, F.; Moreira, I. de P. R.; de Graaf, C.; Barone, V. *Theor. Chem. Acc.* **2000**, *104*, 265. (b) Adamo, C.; Barone, V.; Bencini, A.; Broer, R.; Filatov, M.; Harrison, N. M.; Illas, F.; Malrieu, J. P.; Moreira, I. de P. R. *J. Chem. Phys.* **2006**, *124*, 107101.
(19) (a) Ruiz, E.; Alvarez, S.; Cano, J.; Polo, V. *J. Chem. Phys.* **2005**, *123*, 164110. (b) Ruiz, E. *Struct. Bond.* **2004**, *113*, 71. (c) Ruiz, E.; Alvárez, S.; Rodríguez-Fortea, A.; Alemany, P.; Pouillon, Y.; Massobrio, C. In *Magnetism: Molecules to Materials*; Miller, J. S., Drillon, M., Eds.; Wiley-VCH: Weinheim, Germany, 2001; Vol. 2, p 227.
(20) (a) Wittbrodt, J. M.; Schlegel, H. B. *J. Chem. Phys.* **1996**, *105*, 6574. (b) Goldstein, E.; Beno, B.; Houk, K. N. *J. Am. Chem. Soc.* **1996**, *118*, 6036. (c) Rodriguez, J. H.; Wheeler, D. E.; McCusker, J. K. *J. Am. Chem. Soc.* **1998**, *120*, 12051.
(21) For a recent review, see Yamanaka, S.; Takeda, R.; Shoji, M.; Kitagawa, Y.; Honda, H.; Yamaguchi, K. *Int. J. Quantum Chem.* **2005**, *105*, 605.
(22) Sinnecker, S.; Neese, F.; Noodleman, L.; Lubitz, W. *J. Am. Chem. Soc.* **2004**, *126*, 2613.

Table 2. Selected Bond Distances (Angstroms) and N−Cu−M−N Torsional Angles (Degrees) Observed and Computed for **1** (M = Pd) and **2** (M = Pt)

	1		2	
	observed	computed	observed	computed
M−Cu(1)	2.4971(3)	2.553	2.5016(8)	2.568
M−Cu(2)	2.5022(3)	2.553	2.5053(8)	2.568
M−N[a]	2.010(2)	2.042	2.006(5)	2.043
Cu−N[a]	2.096(2)	2.124	2.104(5)	2.135
Cu(1)−Cl(1)	2.4387(7)	2.548	2.4117(19)	2.548
Cu(2)−Cl(2)	2.4752(7)	2.548	2.4510(18)	2.548
N−Cu−M−N[a]	20.8	18.0	20.7	17.8

[a] Observed values have been averaged.

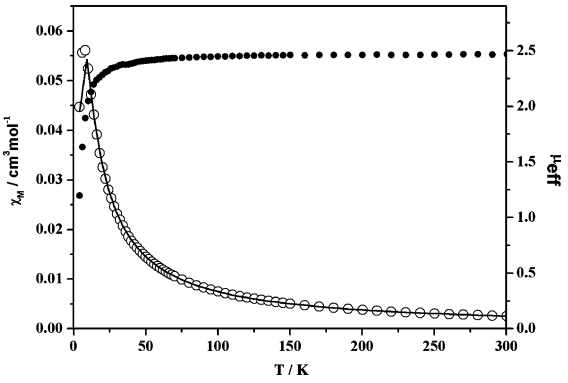

Figure 2. Plot of μ_{eff} (●) and χ_m (○) versus T for **1**. The solid line represents the best theoretical fit.

Cu−N bond lengths of ∼2.10 for **1** and **2** (Table 2) and 2.06 Å for **3**. These Cu−N distances are significantly longer than the central M−N distances (2.01 for **1** and **2** and 1.885 Å for **3**) and are indicative of the presence of unpaired electrons in the orbitals of the outermost metals, which are antibonding with respect to the equatorial ligands. By contrast, the short M−N distances at the central atom suggest a closed-shell d^8 electronic configuration for M. These expectations are confirmed by DFT calculations. In **1** as in **2**, the two Cu−Cl distances differ by ∼0.04 Å, suggesting the existence of nonsymmetric intermolecular interactions. The Cu−M bonds are very close to 2.50 Å for all three complexes. Even though these distances are quite compatible with a metal−metal bond, neither the electron count associated with the metal framework, nor the DFT calculations support the existence of such an interaction.

Magnetic Properties. Magnetic susceptibility measurements for **1** and **2** were made on polycrystalline samples in the temperature range 4−300 K. Temperature-dependent molar magnetic susceptibility (χ_m) and magnetic moment (μ_{eff}) are displayed for **1** and **2** in Figures 2 and 3, respectively.

The μ_{eff} value for **1** is ca. 2.47 μ_B at 300 K and remains constant down to 100 K. This value is similar to that obtained with two independent Cu(II) metal centers (ca. 2.45 μ_B). Below 100 K, μ_{eff} decreases gradually to reach a value of 1.19 μ_B at 4 K. This pattern suggests the presence of an antiferromagnetic coupling between the two Cu(II) metal centers. The corresponding plot of χ_m versus T is also typical of an antiferromagnetic behavior. The χ_m reaches a maximum at 8 K and decreases at lower temperature. An analysis of

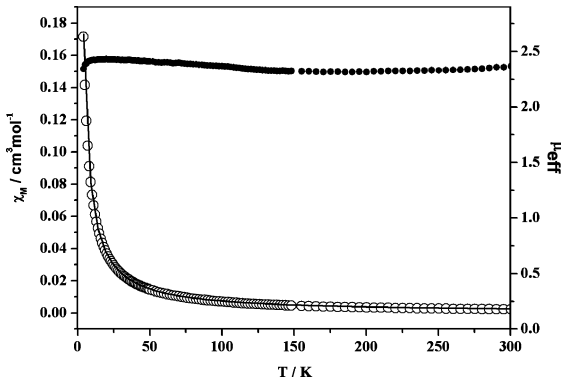

Figure 3. Plot of μ_{eff} (●) and χ_m (○) versus T for **2**. The solid line represents the best theoretical fit.

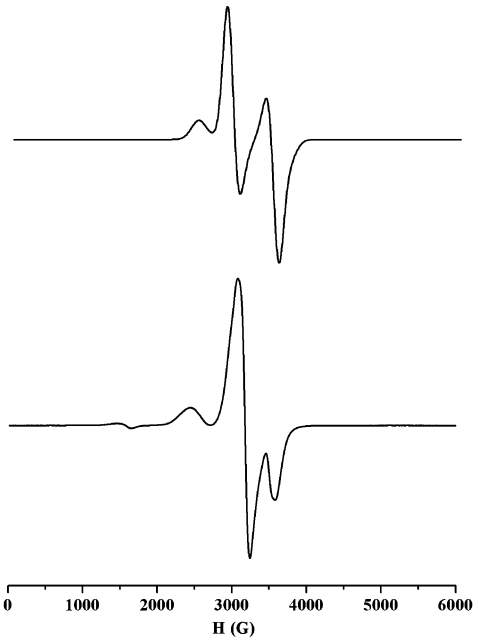

Figure 4. Powder X-band EPR spectrum of **1** at 4 K (bottom) with simulated spectrum (top).

χ_m was carried out using the Bleaney−Bowers equation,[23] using the HDVV Hamiltonian defined in (1):

$$\chi_m = \frac{2Ng^2\beta^2}{kT[3 + \exp(-2J/kT)]} \quad (3)$$

where T is the absolute temperature, and the N, β, and k constants have their usual meanings. The results of the best fit, shown as the solid line in Figure 2 were $g = 2.02$ and $2J = -7.45$ cm^{-1}, showing a weak antiferromagnetic coupling.

The magnetic behavior of **2** (Figure 3) is different from that of **1**. The μ_{eff} value is nearly constant except below 7 K, where it decreases slightly. This suggests that the exchange interaction between the two Cu(II) ions is particularly weak. The least-square fitting of the χ_m value with eq 1 confirms this prediction by leading to $g = 2.00$ and $2J = -0.77$ cm^{-1}.

Figures 4 and 5 display the powder electron paramagnetic resonance (EPR) spectra obtained at 4 K for **1** and **2**. Both

(23) Bleaney, B.; Bowers, K. D. *Proc. R. Soc. London, Ser. A* **1952**, *214*, 451.

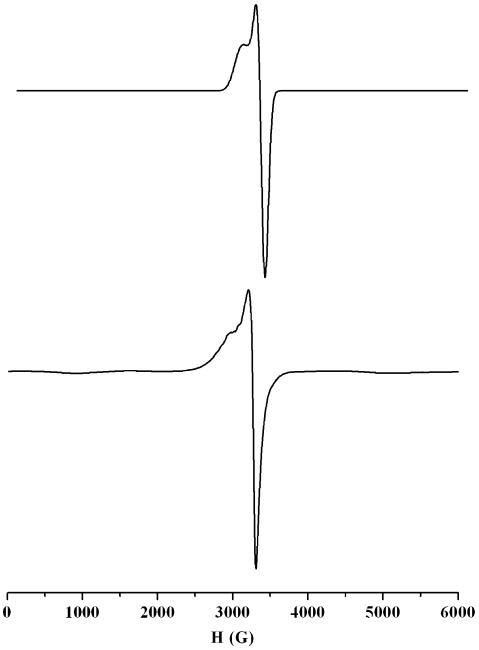

Figure 5. Powder X-band EPR spectrum of **2** at 4 K (bottom) with simulated spectrum (top).

of them display an axially symmetric EPR pattern ($g_{||} > g_{\perp}$). These features are indicative of a $\{d_{x^2-y^2}\}$ ground state and a distorted square pyramidal or octahedral geometry at the magnetically isolated copper(II) centers, which is in keeping with the X-ray crystallographic analysis.

For **1**, the EPR spectrum displays a sharp $g_{\perp}$ band centered at 3180 G and a pair of $g_{||}$ bands at 2435 and 3575 G. Another weak signal can be observed at ca. 1560 G, which is the spin-forbidden $|\Delta Ms| = 2$ (double quantum line) feature. From the magnetic results of **1**, the excited triplet state is destabilised by -7.45 cm^{-1} within the thermal accessible range of *kT* values. Thus, the EPR transitions of **1** should be discussed by considering both the singlet ground state and the triplet excited state. The double quantum line is expected to arise from the $|1,-1\rangle \rightarrow |1,1\rangle$ transition, involving levels of the triplet state. It is therefore consistent with a weak magnetic coupling between the Cu(II) ions. A similar pattern was indeed found in some binuclear copper(II) complexes exhibiting weak coupling, either ferro- or antiferromagnetic.[24] Between 2000 and 4000 G, the $|\Delta Ms| = 1$ peaks could be assigned to the singlet−triplet transitions *and* to the transitions within the triplet states.[25] These EPR features are consistent with those of binuclear copper(II) complexes, displaying *weak antiferromagnetic* interaction.[24c,26] A qualitative simulation of the EPR spectrum of **1**, was carried out by means of the *WINEPR-Simfonia* software,[27] assuming an axially symmetric triplet state (Figure 4, top). The calculated EPR parameters are $g_z = 2.25$, $g_x = g_y = 2.1$, and $D = 0.06$ cm^{-1}. However, the intense signal observed at ca. $g = 2$ could not be simulated successfully, probably due to the singlet-to-triplet transitions, which could not be modeled by *WINEPR-Simfonia*.[27]

The EPR spectrum of **2** (Figure 5) consists of one asymmetric band centered at $g_{\perp} = 2.07$ and a second band with less resolution at $g_{||} = 2.28$, which seems indicative of a triplet state. This is consistent with the magnetic measurements, concluding to a very weak antiferromagnetic interaction ($2J = -0.77$ cm^{-1}). The singlet and the triplet states are therefore nearly degenerate, and a significant population of the triplet state can be expected, even at 4K. Similar EPR spectra have been observed previously in various dicopper(II) complexes, exhibiting various kinds of weak or very weak couplings, either antiferromagnetic or ferromagnetic.[28,29] In the present case, no clear resonance is detected in the $|\Delta Ms| = 2$ region, which is indicative of a very weak zero-field splitting.[29c] The simulated EPR spectrum of **2**,[27] (Figure 5) using $g_z = 2.28$, $g_x = g_y = 2.07$, and $D = 0.003$ cm^{-1}, is in good agreement with the experimental data.

DFT Calculations. Interatomic distances obtained from geometry optimization, separately carried out on the high spin state and on the broken symmetry solution, differ by less than 1 picometer for **1** as for **2**. Computed geometries referred to in Table 2 and used for the calculation of the magnetic coupling coefficient 2*J* are those corresponding to the high spin state. These geometries are quite similar for both complexes and in correct agreement with crystal structures, except for Cu−Cl distances, which are overestimated by ∼0.11 Å, in average. This overestimation should be assigned in part to the lack of polarization functions in the basis set, but the differences observed in each complex between the two Cu−Cl distances suggest that intermolecular interactions are at work to modify the position of chlorine atoms.

The energy difference ${}^{BS}E - {}^{T}E$ between both calculated spin states is in favor of the broken symmetry solution for **1** as for **2**, and the computed coupling is therefore antiferromagnetic. The energy differences are quite similar for both complexes, and the values of $-2J$ calculated by means of Yamaguchi's approximate projection formula are 14.3 and 16.5 cm^{-1} for **1** and **2**, respectively.[30] The coupling constant calculated previously with the same atomic basis sets for the isoelectronic complex $[Cu_3(dpa)_4Cl_2]^+$ (**3**) was $-2J =$

(24) (a) Geetha, K.; Nethaji, M.; Chakravarty, A. R.; Vasanthacharya, N. Y. *Inorg. Chem.* **1996**, *35*, 7666. (b) Tolman, W. B.; Rardin, R. L.; Lippard, S. J. *J. Am. Chem. Soc.* **1989**, *111*, 4532. (c) Davis, W. M.; Lippard, S. J. *Inorg. Chem.* **1985**, *24*, 3688.
(25) Bencini, A.; Gatteschi, D. *EPR of Exchange Coupled Systems*; Springer-Verlag: Berlin, 1990.
(26) (a) Coughlin, P. K.; Lippard, S. J. *Inorg. Chem.* **1984**, *23*, 1446. (b) Bencini, A.; Gatteschi, D.; Reedijk, J.; Zanchini, C. *Inorg. Chem.* **1985**, *24*, 207. (c) Folgado, J. V.; Ibáñez, R.; Coronado, E.; Beltrán, D.; Savariault, J. M.; Galy, J. *Inorg. Chem.* **1988**, *27*, 19.
(27) *WINEPR SIMFONIA, Version 1.25*; Brüker Analytische Messtechnik: Germany, 1996.
(28) Rodriguez, M.; Llobet, A.; Corbella, M.; Martell, A. E.; Reibenspies, J. *Inorg. Chem.* **1999**, *38*, 2328.
(29) (a) Villa, J. F.; Hatfield, W. E. *Inorg. Chem.* **1972**, *11*, 1331. (b) Kapoor, P.; Pathak, A.; Kapoor, R.; Venugopalan, P.; Corbella, M.; Rodríguez, M.; Robles, J.; Llobet, A. *Inorg. Chem.* **2002**, *41*, 6153. (c) Lucas, R.; Liu, S.; Thompson, L. K. *Inorg. Chem.* **1990**, *29*, 85. (d) Verdaguer, M.; Gouteron, J.; Jeannin, S.; Jeannin, Y.; Kahn, O. *Inorg. Chem.* **1984**, *23*, 4291. (e) Castiñeiras, A.; Domínguez, R.; Gómez-Rodríguez, L.; Borrás, J. *Z. Anorg. Allg. Chem.* **2003**, *629*, 1096. (f) Castiñeiras, A.; Balboa, S.; Bermejo, E.; Carballo, R.; Covelo, B.; Borrás, J.; Real, J. A. *Z. Anorg. Allg. Chem.* **2002**, *628*, 1116.
(30) Calculations were carried out at the same level of theory on the hypothetic and isoelectronic complex $NiCu_2(dpa)_4Cl_2$ yield a magnetic coupling constant with similar order of magnitude, $-2J = 10.9$ cm^{-1}.

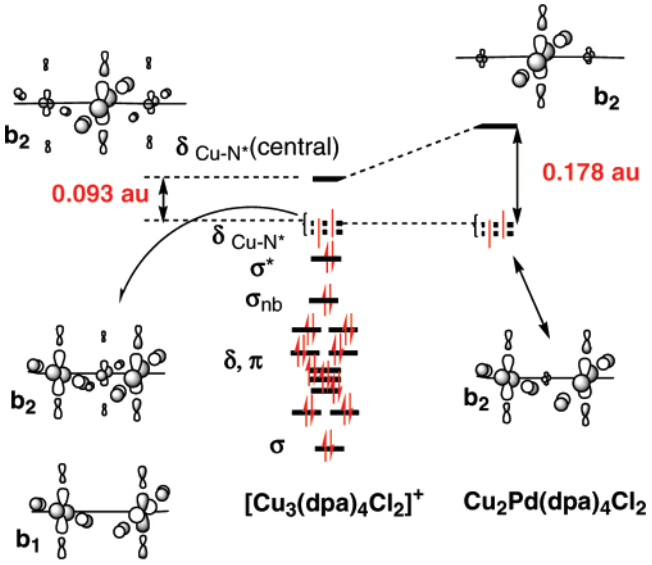

Figure 6. Sequence and occupancies of the metal orbitals in $[Cu−M−Cu(dpa)_4Cl_2]^{0,1+}$ complexes with 26 metal electrons and evolution of the energy gap between the highest partly occupied and the lowest unoccupied MOs from $[Cu_3(dpa)_4Cl_2]^+$ to heterotrimetallic complexes such as $Cu_2Pd(dpa)_4Cl_2$.

64 cm^{-1}.[31] The values of $-2J$ calculated for copper/palladium complex **1** and for **3**[10] are both overestimated by a factor of ∼2.[32] Experiment and calculations therefore agree on the fact that the replacement of central copper in **3** by palladium reduces the magnetic interaction by a factor of ∼4. According to magnetic measurements and EPR spectra, the presence of platinum in the central position induces a further collapse of the magnetic interaction, which is not accounted for by the present level of calculations. It is suggested that spin−orbit interactions generated by the heavy metal contribute to modify the magnetic behavior of **2.** A reliable investigation of spin−orbit effects is clearly beyond the scope of the present work, on the basis of DFT calculations. It indeed requires a balanced treatment of spin−orbit splitting and electron correlation within an appropriate ab initio post-Hartree−Fock treatment. We will therefore restrict the present discussion to the modifications induced by Pd(II) with respect to Cu(III).

DFT calculations are in agreement with the interpretation of crystal structures to assign the ionization process in $[Cu_3(dpa)_4Cl_2]^+$ to the removal of an electron accommodated on the δ orbital highest in energy,[31] displaying its major weight on the central copper and an antibonding character with respect to the four surrounding nitrogen atoms (Figure 6). The central copper atom can therefore be formally assigned the oxidation state III and a d^8 population, same as for Pd(II) in **1**. **1** and **3** are also isostructural, and the square planar environment of the central metal in both cases is in keeping with their low spin electronic configuration. Neither $Cu_{central}$ in **3** or palladium in **1** are magnetic centers, but both

(31) Bénard, M.; Berry, J. F.; Cotton, F. A.; Gaudin, C.; López, X.; Murillo, C. A.; Rohmer, M.-M. *Inorg. Chem.* **2006**, *45*, 3932.
(32) It was noted by a reviewer of ref 31 that the use of unprojected values, as recommended by some authors (ref 19), would yield an excellent agreement with observation.

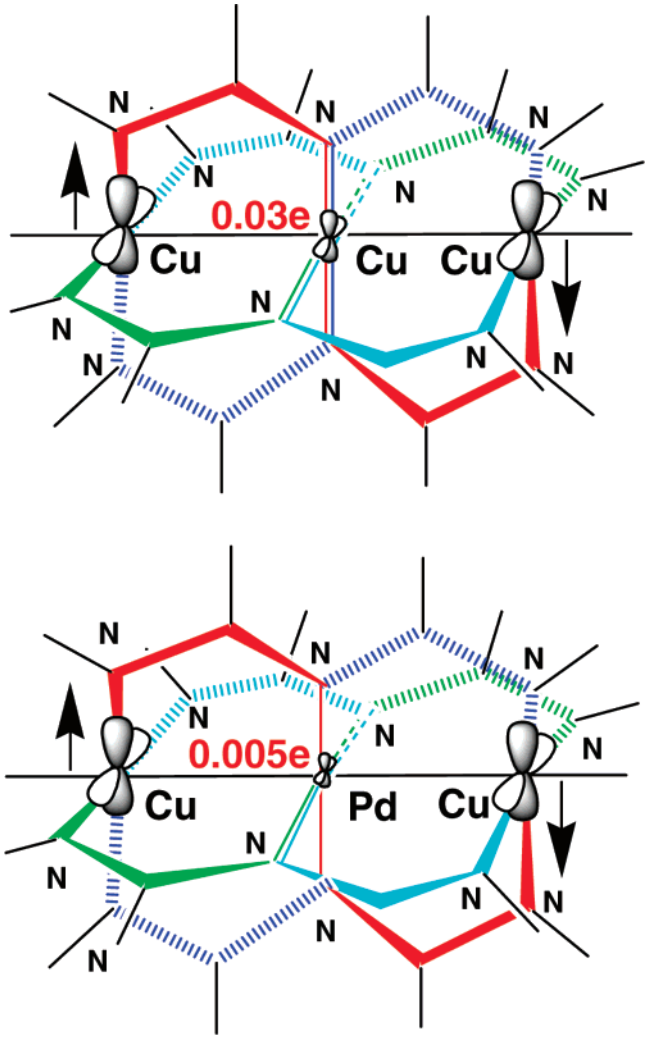

Figure 7. Spin populations (electrons) at the crossing point of the four superexchange pathways of $[Cu_3(dpa)_4Cl_2]^+$ and $Cu_2Pd(dpa)_4Cl_2$.

are at the crossing point of the superexchange interaction coupling the outermost Cu(II) magnetic centers via the four dpa ligands (Figure 7). The superexchange pathways are initialized by the antibonding interaction involving the two magnetic centers and their equatorial ligand environment. Then, the propagation of the superexchange depends on two critical sections: (i) the contact between adjacent nitrogens belonging to the coordination sphere of a terminal metal and of the central metal, respectively, and (ii) the transmission of the superexchange interaction at the crossing point of the four pathways, namely at the central metal.

It is clear that a through-bond transmission of the superexchange interaction via the pyridine carbons comes up against the very low distribution of the spin density along the carbon framework. This density even becomes slightly negative at the bridging carbon atom, indicative of a polarization mechanism. Gutiérrez et al., however, reported a similar situation in a series of bridged dinuclear complexes of Cu(II) and did not exclude the possibility of through-space delocalization of the spin density between the ligand environment of neighboring metals.[33] In the present case, this hypothesis appears in agreement with the calculated sensitivity of the J coupling constant with the torsional angle

of the dpa ligand. In the geometry optimized for **1**, the N−Cu−Pd−N angle is 18.0° (Table 2). Constraining this angle to the observed value of 20.8° and reoptimizing the rest of the structure decreases $-2J$ from 14.3 to 13.2 cm^{-1}. A further increase of the torsional angle to 30° yields $-2J = 10.6$ cm^{-1}. The same trend was obtained when the Cu−Pd and the metal−nitrogen distances were also constrained to their observed values: $-2J$ then decreases from 13.8 cm^{-1} for a torsional angle of 20.8° to 10.5 cm^{-1} for a torsional angle of 30°. This consistent decrease, also calculated for **2**, contrasts with a remarkable insensitivity of J with respect to changes in the Cu−M or in the Cu−N and M−N distances.[34] This weakening of the magnetic coupling when the helical trend of the ligand coating increases could be assigned to a more-difficult through-space contact between external and internal nitrogens.

The next crucial part of the superexchange pathways lies at the crossing point of the four bridging ligands, namely at the nonmagnetic metal center, either Cu(III), Pd(II), or Pt(II). In a previous study of **3**, we noticed that the computed fluctuations of the antiferromagnetic coupling as a function of various geometrical parameters could be correlated with the amount of spin density assigned to the $d_{x^2-y^2}$ orbital of the central metal in the molecular high spin state.[31] The present work confirms that the spin delocalization along the directions of the central M−N bonds appears as a key factor to the strength of the superexchange process. The spin density at the central metal indeed arises from the semi-occupied MO with b_2 symmetry (follow arrows in Figure 6). This orbital is mainly localized on the two magnetic centers, but some density settles down at the central site, arising from the contamination of the highest unoccupied δ orbital of same symmetry (Figure 6). The importance of that contamination depends on the energy gap between the two MOs with b_2 symmetry: the lower the gap, the larger the spin density at the central site. For the tricopper cation, the gap originates in the stronger donation interaction induced by the more-basic amido ligands, compared with pyridines. It amounts to 0.093 au (2.53 eV), and the spin population on the $d_{x^2-y^2}$ orbital of $Cu_{central}$ is 0.031 electrons (Figures 6 and 7). When copper is replaced by palladium or platinum, however, the energy gap also incorporates the difference between intrinsic energies assigned to the outer d shells of the metal atoms. This energy is obviously deeper for copper, for which the d shell is often considered as accommodating semi-core electrons. Moreover, the donation interaction from the ligand appears stronger with palladium than with copper, which raises the energy of the M−N antibonding counterpart further. The SOMO−LUMO gap for **1** therefore increases to 0.178 au (4.84 eV), and the spin population along the $(Cu-N)_{central}$ direction drops to 0.005 electron (Figures 6 and 7), making the transference of the superexchange interaction much more difficult.

Conclusion and Perspectives. After $Co_2Pd(dpa)_4Cl_2$,[9] the synthesis of $Cu_2Pd(dpa)_4Cl_2$ and $Cu_2Pt(dpa)_4Cl_2$ extends the scope of Extended Metal Atom Chains (EMACs) toward novel properties, arising from the contact between different types of transition-metal atoms. Comparing the properties of the new compounds with those of the homonuclear, isoelectronic homolog $[Cu_3(dpa)_4Cl_2]^+$ (**3**), provides indications on the changes that can be expected from heteronuclearity. First, the change does not affect *in the present case* the structural pattern observed in most $M_3(dpa)_4L_2$ complexes, namely, the linearity of the framework made of metal atoms and axial ligands, and the helical shape of the dpa coating. The near-identity of the metal−metal distances observed in **1** and **2**, leading to an approximate D_4 molecular symmetry, presents notable exceptions in the $M_3(dpa)_4L_2$ family but conforms to the structure of **3**. In spite of the structural and electronic similarity between **1**, **2**, and **3**, notable differences are observed, however, concerning the temperature-dependent magnetic behavior and the EPR spectra. The replacement in the central position of a diamagnetic Cu(III) by a diamagnetic Pd(II) decreases by a factor of ~4 the superexchange interaction between the two outermost Cu(II) atoms. This interaction is almost cancelled in **2**. The weakening of $-2J$ observed in **1** can be reproduced by DFT calculations, which emphasize the role of the nonmagnetic metal in the superexchange process. However, no decisive rationalization can be proposed at that level of theory for the annihilation of the magnetic interaction observed in **2**. This fine tuning of the magnetic behavior in a series of isostructural and isoelectronic compounds appears promising in the perspective of using such building blocks with controlled properties for future electronic applications. Still-deeper changes should be expected in the near future from the characterization of new heteronuclear EMACs with unprecedented metal electron counts and also from that of nonsymmetric isomers of the present complexes.

Acknowledgment. The authors acknowledge the CNRS, the Ministère de l'Education Nationale, de l'Enseignement Supérieur et de la Recherche (MENESR, Paris, France), the National Science Council, and the Ministry of Education of Taiwan for financial support. Calculations have been shared between the IDRIS (CNRS, Orsay, France), the CINES (Montpellier, France), and the NCHC (Taipei, Taiwan) computer centers.

Supporting Information Available: Plot of the molecular structure of **2**; total energies, symmetry constraints, optimized Cartesian coordinates, Mulliken charges, atomic spin populations obtained from DFT/UB3LYP calculations carried out on the high-spin ground states of **1** and **2**. X-ray crystallographic files are available for **1**·$(C_2H_5)_2O$ and **2**·$(C_2H_5)_2O$. This material is available free of charge via the Internet at http://pubs.acs.org.

IC070319L

(33) Gutiérrez, L.; Alzuet, G.; Borrás, J.; Castiñeiras, A.; Rodríguez-Fortea, A.; Ruiz, E. *Inorg. Chem.* **2001**, *40*, 3089.

(34) An elongation of the Cu−Pd distance by 0.1 Å in **1** yields a decrease of $-2J$ by 1.1 cm^{-1}. In the same complex, an elongation of all metal−nitrogen distances by 0.05 Å increase the strength of the coupling by 1.3 cm^{-1}. Similar trends have been obtained with **2**.